STEERABLE FILTERS FOR ORIENTATION ESTIMATION AND LOCALIZATION OF FLUORESCENT DIPOLES

François Aguet[1], *Stefan Geissbühler*[1,2], *Iwan Märki*[2], *Theo Lasser*[2] *and Michael Unser*[1]

[1]Biomedical Imaging Group, [2]Biomedical Optics Group
Ecole Polytechnique Fédérale de Lausanne, Switzerland

ABSTRACT

Fluorescence localization microscopy (i.e., PALM, STORM) has enabled optical imaging at nanometer-scale resolutions. The localization algorithms used in these techniques rely on fitting a 2-D Gaussian to the in-focus image of individual fluorophores. For fixed fluorophores, however, the observed diffraction pattern depends on the orientation of the underlying molecular dipole and does not necessarily correspond to a section of the system's point spread function. By using a physically realistic image formation model for dipoles to perform the fit, both the position and orientation of the dipole can be estimated with high accuracy, improving upon Gaussian localization. In this paper, we present an algorithm for joint position and orientation estimation based on a 3-D steerable filter, and show that the results are near-optimal with respect to the Cramér-Rao bounds. We show that patterns generated using estimated positions and orientations closely fit experimental measurements.

Index Terms— Fluorescence microscopy, Fluorescent dipoles, Localization, Steerable filters, Superresolution

1. INTRODUCTION

The fluorescence localization microscopy techniques introduced in recent years have enabled optical imaging of complex specimens at molecular resolutions, down to the nanometer scale. Most of these techniques, such as photoactivated localization microscopy (PALM) [1] and stochastic optical reconstruction microscopy (STORM) [2], are best suited to imaging 2-D sections of thin, fixed specimens. Accordingly, the images of individual molecules are assumed to correspond to the in-focus section of the microscope's 3-D point spread function (PSF), which can be approximated by a 2-D Gaussian function without significant loss in lateral localization accuracy [3]. In this approach, any molecule within the depth of field of the system can be detected and localized, meaning that the axial resolution of the resulting image can be of the order of several hundred nanometers (for an objective with a high numerical aperture (NA)).

This work was supported by the Swiss National Science Foundation under grant 200020-109415, as well as by the Hasler foundation under grant 2033.

The lateral localization accuracies that are claimed for these super-resolution techniques are usually based on the assumption that individual fluorophores in the sample act as isotropically emitting point sources, and thus, that their image corresponds to a section of the system's PSF [4]. While this is valid for fluorophores that freely rotate during image acquisition, it does not hold for fixed fluorophores. Their corresponding diffraction patterns are significantly different and highly specific of the orientation of the fluorophore's underlying dipole. Even when imaged in focus, the observed intensity maximum corresponding to such a dipole may be shifted by several nanometers with respect to the absolute position of the fluorophore, inducing a significant bias in the localization [5].

In order to address the lack of depth discrimination, extensions of STORM to 3-D involving cylindrical optics have been proposed (see, e.g., [6]). However, these approaches require a specimen-specific calibration, and are also subject to producing biased results when applied to fluorescent dipoles. A solution to avoiding this bias in all instances is to use an approach based on an accurate image formation model for dipoles, where the localization is performed by numerically fitting this model to observations. In comparison to PSF-based localization approaches [7], this introduces additional degrees of freedom in the form of dipole orientation parameters. In this work, we show that image formation for dipoles can be decomposed into six non-orthogonal basis functions, which may be used to formulate the orientation estimation problem as the optimization of a 3-D steerable filter [8]. The resulting algorithm serves both as method to obtain an initial detection with localization at the pixel level, and as an efficient means of updating the orientation estimates when performing the subsequent sub-pixel localization to achieve super-resolution.

2. IMAGE FORMATION FOR DIPOLES

A single fluorophore can be described as a harmonically oscillating dipole characterized by a position $\boldsymbol{x}_p = (x_p, y_p, z_p)$ and a moment $\mathbf{p} = (\sin\theta_p \cos\phi_p, \sin\theta_p \sin\phi_p, \cos\theta_p)$, where θ_p is the zenith angle (i.e., between the dipole and the optical axis) and ϕ_p is the azimuth angle. The diffraction pattern observed

when imaging such a dipole may be written as

$$\begin{aligned} h_{\theta_p,\phi_p}(\boldsymbol{x};\boldsymbol{x}_p,\boldsymbol{\tau}) = \\ &\sin^2\theta_p\Big(|I_0|^2+|I_2|^2+2\cos(2\phi_p-2\phi_d)\Re\{I_0^*I_2\}\Big) \\ &-2\sin(2\theta_p)\cos(\phi_p-\phi_d)\Im\{I_1^*(I_0+I_2)\} \\ &+4|I_1|^2\cos^2\theta_p \\ &=\mathbf{p}^\mathsf{T}\mathbf{M}\mathbf{p}, \end{aligned} \tag{1}$$

where $\phi_d = \tan^{-1}\big((y-y_p)/(x-x_p)\big)$. An asterisk denotes complex conjugation, and $\boldsymbol{v}^\mathsf{T}$ stands for the Hermitian transpose of $\boldsymbol{v}$. The symmetric matrix $\mathbf{M}=(m_{ij})_{1\leqslant i,j\leqslant 3}$ is specified by

$$\begin{aligned} m_{11} &= |I_0|^2+|I_2|^2+2\Re\{I_0^*I_2\}\cos 2\phi_d \\ m_{12} &= 2\Re\{I_0^*I_2\}\sin 2\phi_d \\ m_{13} &= -2\cos\phi_d\Im\{I_1^*(I_0+I_2)\} \\ m_{22} &= |I_0|^2+|I_2|^2-2\Re\{I_0^*I_2\}\cos 2\phi_d \\ m_{23} &= -2\sin\phi_d\Im\{I_1^*(I_0+I_2)\} \\ m_{33} &= 4|I_1|^2. \end{aligned} \tag{2}$$

The integral expressions for I_0, I_1, and I_2 are given by

$$\begin{aligned} &I_0(\boldsymbol{x};\boldsymbol{x}_p,\boldsymbol{\tau}) \\ &\quad=\int_0^\alpha B_0(\theta)\Big(t_s^{(1)}t_s^{(2)}+t_p^{(1)}t_p^{(2)}\frac{1}{n_s}\sqrt{n_s^2-n_i^2\sin^2\theta}\Big)\,\mathrm{d}\theta \\ &I_1(\boldsymbol{x};\boldsymbol{x}_p,\boldsymbol{\tau}) \\ &\quad=\int_0^\alpha B_1(\theta)t_p^{(1)}t_p^{(2)}\frac{n_i}{n_s}\sin\theta\,\mathrm{d}\theta \\ &I_2(\boldsymbol{x};\boldsymbol{x}_p,\boldsymbol{\tau}) \\ &\quad=\int_0^\alpha B_2(\theta)\Big(t_s^{(1)}t_s^{(2)}-t_p^{(1)}t_p^{(2)}\frac{1}{n_s}\sqrt{n_s^2-n_i^2\sin^2\theta}\Big)\,\mathrm{d}\theta, \end{aligned} \tag{3}$$

where

$$B_m(\theta)=\sqrt{\cos\theta}\sin\theta J_m(krn_i\sin\theta)\mathrm{e}^{ik\Lambda(\theta,z,z_p,\boldsymbol{\tau})}. \tag{4}$$

For conciseness, the arguments are omitted from the notation of these functions whenever they are explicit from the context. The phase component $\Lambda(\theta,z,z_p,\boldsymbol{\tau})$ describes the system's aberrations due to defocus, index mismatches etc., and the parameter vector $\boldsymbol{\tau}=(\mathrm{NA},\mathbf{n},\mathbf{t})$ contains the optical parameters of the system: NA, refractive index $\mathbf{n}$ and thickness $\mathbf{t}$ of the specimen, glass, and immersion layers in the sample setup [9, 10].

2.1. Noise model

In single molecule fluorescence microscopy, shot noise induced by fluorescence emission in the sample is the dominant source of noise. In addition to the signal of interest, it depends on the contributions of potential background terms, such as residual signals from other fluorophores and autofluorescence of the sample. Additionally, read-out noise in the detector may also be a factor. Unlike shot noise, which obeys Poisson statistics, read-out noise is Gaussian-distributed. Given that the Poisson distribution rapidly converges towards a Gaussian with equal mean and variance when the variance is large enough (this is usually considered the case when $\sigma^2>10$), we propose a general noise model consisting of a shifted Poisson formulation that incorporates a term accounting for the read-out noise factor and background. Consequently, we formulate the expected photon count $\bar{q}(\boldsymbol{x};\boldsymbol{x}_p,\boldsymbol{\tau})$ corresponding to a point $\boldsymbol{x}$ on the detector (in object-space coordinates) as

$$\bar{q}(\boldsymbol{x};\boldsymbol{x}_p,\boldsymbol{\tau})=c\cdot\big(A\,h_{\theta_p,\phi_p}(\boldsymbol{x};\boldsymbol{x}_p,\boldsymbol{\tau})+b\big), \tag{5}$$

where A is the amplitude, c is a conversion factor, and b is the sum of the background fluorescence signal and the variance σ_r^2 (in intensity) of the read-out noise. The probability of detecting q photons at $\boldsymbol{x}$ is then given by

$$P_{\bar{q}(\boldsymbol{x};\boldsymbol{x}_p,\boldsymbol{\tau})}(q)=\frac{\mathrm{e}^{-\bar{q}(\boldsymbol{x};\boldsymbol{x}_p,\boldsymbol{\tau})}\bar{q}(\boldsymbol{x};\boldsymbol{x}_p,\boldsymbol{\tau})^q}{q!}. \tag{6}$$

3. STEERABLE FILTERS

A standard approach to estimating the position and orientation of arbitrarily rotated image features—such as the dipole diffraction patterns discussed in this work—consists in correlating the input data with a set of templates that correspond to rotated versions of the expected feature. The quadratic form (1) shows that the 3-D rotation of a dipole can be decoupled from filtering, i.e., that the orientation and position estimation can be expressed as a 3-D steerable filter (for localization at the pixel level). Similarly to the steerable filters introduced by Freeman and Adelson [8], the dipole diffraction pattern can be decomposed into six templates weighted by trigonometric interpolation functions, as illustrated in Fig. 1. An example of these templates is shown in Fig. 2.

A suitable decomposition is obtained by formulating the orientation and position estimation problem using the least-squares criterion

$$\begin{aligned} J_{\mathrm{LS}}(\boldsymbol{x};\theta_p,\phi_p) &= \int_\Omega\big(Ah_{\theta_p,\phi_p}(\boldsymbol{v};\boldsymbol{x}_p,\boldsymbol{\tau})-f(\boldsymbol{x}-\boldsymbol{v})\big)^2\,\mathrm{d}\boldsymbol{v} \\ &= \big\|Ah_{\theta_p,\phi_p}(\boldsymbol{x};\boldsymbol{x}_p,\boldsymbol{\tau})\big\|^2+\int_\Omega f(\boldsymbol{x}-\boldsymbol{v})^2\,\mathrm{d}\boldsymbol{v} \\ &\quad-2Ah_{\theta_p,\phi_p}(\boldsymbol{x};\boldsymbol{x}_p,\boldsymbol{\tau})*f(\boldsymbol{x}), \end{aligned} \tag{7}$$

where $f(\boldsymbol{x})$ is the observed signal from which the estimated value b has been subtracted, and where $\Omega\subset\mathbb{R}^2$ is the support of h_{θ_p,ϕ_p}. The correlation term is steerable and can be expressed as

$$\begin{aligned} \big(h_{\theta_p,\phi_p}*f\big)(\boldsymbol{x}) &= \sum_{ij}a_{ij}(\phi_p,\theta_p)\big(m_{ij}*f\big)(\boldsymbol{x}) \\ &=\mathbf{p}^\mathsf{T}\mathbf{M}_f\mathbf{p}, \end{aligned} \tag{8}$$

where $a_{ij}(\theta_p, \phi_p)$ are the weighting functions given in Fig. 1, and where $[\mathbf{M}_f]_{ij} = m_{ij} * f$. The model energy term is independent of ϕ_p and can be rewritten as

$$\left\| A h_{\theta_p,\phi_p}(\boldsymbol{x}; \boldsymbol{x}_p, \boldsymbol{\tau}) \right\|^2 = A^2 \mathbf{u}_{\theta_p}^{\mathsf{T}} \mathbf{E} \mathbf{u}_{\theta_p}, \tag{9}$$

where $\mathbf{u}_{\theta_p} = (\sin^2\theta_p, \sin 2\theta_p, \cos^2\theta_p)^{\mathsf{T}}$, and where $\mathbf{E}$ is defined as

$$\mathbf{E} = \begin{bmatrix} \langle m_{11}^2 \rangle & \langle m_{11} m_{13} \rangle & \langle m_{11} m_{33} \rangle \\ \langle m_{11} m_{13} \rangle & \langle m_{13}^2 \rangle & \langle m_{13} m_{33} \rangle \\ \langle m_{11} m_{33} \rangle & \langle m_{13} m_{33} \rangle & \langle m_{33}^2 \rangle \end{bmatrix}. \tag{10}$$

The notation $\langle m_{ij} \rangle$ stands for integration over the support Ω of $m_{ij}(\boldsymbol{x})$. The optimization of (7) is independent of the data term, and the criterion thus simplifies to

$$J(\boldsymbol{x}; \theta_p, \phi_p) = A^2 \mathbf{u}_{\theta_p}^{\mathsf{T}} \mathbf{E} \mathbf{u}_{\theta_p} - 2A \mathbf{p}^{\mathsf{T}} \mathbf{M}_f \mathbf{p}. \tag{11}$$

This function cannot be solved in closed form for θ_p, ϕ_p, and A. However, an iterative algorithm is obtained by setting the partial derivatives

$$\begin{aligned} \frac{\partial}{\partial \theta_p} J(\boldsymbol{x}; \theta_p, \phi_p) &= 2A \left(A \mathbf{u}_{\theta_p}^{\mathsf{T}} \mathbf{E} \frac{\partial}{\partial \theta_p} \mathbf{u}_{\theta_p} - 2 \mathbf{p}^{\mathsf{T}} \mathbf{M}_f \frac{\partial}{\partial \theta_p} \mathbf{p} \right) \\ \frac{\partial}{\partial \phi_p} J(\boldsymbol{x}; \theta_p, \phi_p) &= -2 \mathbf{p}^{\mathsf{T}} \mathbf{M}_f \frac{\partial}{\partial \phi_p} \mathbf{p} \end{aligned} \tag{12}$$

to zero and alternately solving for θ_p and ϕ_p, which is more efficient in comparison to a gradient-based approach. The notation $\frac{\partial}{\partial t}\boldsymbol{v}$ stands for the component-wise derivative of the vector $\boldsymbol{v}$ with respect to t. Between these iterations, the amplitude is updated using the least-squares solution

$$\hat{A} = \frac{\mathbf{p}^{\mathsf{T}} \mathbf{M}_f \mathbf{p}}{\mathbf{u}_{\theta_p}^{\mathsf{T}} \mathbf{E} \mathbf{u}_{\theta_p}}. \tag{13}$$

When all other parameters are known (i.e., $\boldsymbol{x}_p$, and $\boldsymbol{\tau}$), the angles can be estimated in a small number of iterations (usually less than five).

As stated earlier, this approach based on steerable filters results in a pixel-level localization of dipoles. In order to obtain super-resolved position information, further refinement is needed; this is achieved iteratively using a gradient-based approach. The position returned by the steerable filter serves as an initialization to this procedure, during which the angles are also updated. Due to the precise pixel-level estimates, the sub-pixel adjustments are usually fast. A complete description of this algorithm is given in [10].

4. ESTIMATION ACCURACY

The performance of the proposed least-squares orientation estimation method is near-optimal in the sense that the variance of the estimation results essentially reaches the Cramér-Rao

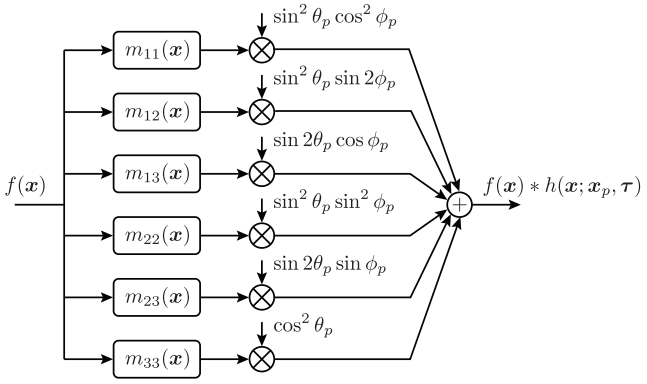

Fig. 1 Filterbank implementation of the steerable dipole filters.

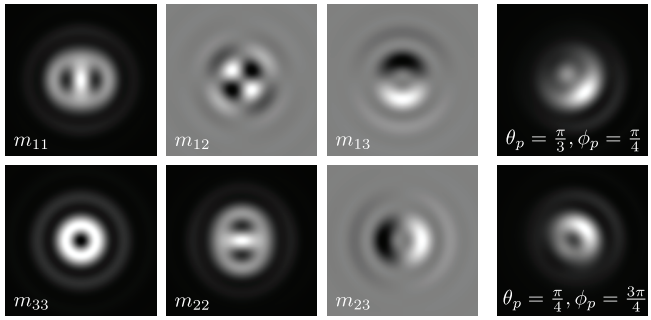

Fig. 2 High-resolution versions of the templates used in the steerable decomposition of dipole diffraction patterns. The example shown is for dipoles at an air/glass interface, imaged with a 100×, 1.45 NA objective at 400 nm defocus.

bounds (CRB) for both angles. These bounds provide a lower bound on the variance of any unbiased estimator; for the angular parameters of a dipole they are given by

$$\begin{aligned} \mathrm{Var}(\hat{\theta}_p) &\geq [\mathbf{F}^{-1}]_{11} \\ \mathrm{Var}(\hat{\phi}_p) &\geq 1 \Big/ \int_\Omega \frac{1}{\bar{q}} \left(\frac{\partial \bar{q}}{\partial \phi_p} \right)^2 \mathrm{d}\boldsymbol{x}, \end{aligned} \tag{14}$$

where the Fisher information matrix for the parameters $\vartheta = (\theta_p, A)$ is specified by

$$\mathbf{F}_{ij} = \int_\Omega \frac{1}{\bar{q}} \frac{\partial \bar{q}}{\partial \vartheta_i} \frac{\partial \bar{q}}{\partial \vartheta_j} \mathrm{d}\boldsymbol{x}. \tag{15}$$

Note that the bound for ϕ_p is independent of the bounds for the other parameters, i.e., the respective cross-components in the Fisher information matrix are zero. In Fig. 3, we compare the standard deviations of the estimated angle values and amplitude from simulated data to the value of the CRB.

5. RESULTS

The localization accuracy achieved in simulation and the CRBs show that it is possible to estimate the orientation of a fluorescent dipole with a precision of a few degrees (see Fig. 3).

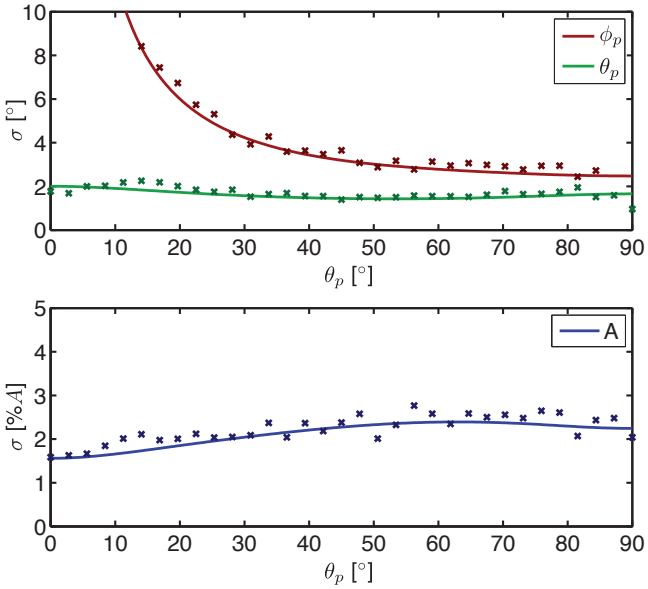

Fig. 3 Performance analysis of the 3-D steerable filter-based estimation of θ_p, ϕ_p, and A. The solid lines correspond to the Cramér-Rao bounds, and the markers correspond to the standard deviation σ of estimation results over 100 experiments using different realizations of noise. Optical parameters: M = 100×, NA = 1.45, n_i = 1.515, n_s = 1.00, λ = 666 nm, z = 400 nm, average peak signal-to-noise ratio at 25 dB, background intensity level: 20%.

We performed preliminary experimental validation of the proposed approach by imaging single Cy5 molecules bound to single-stranded DNA (ssDNA). A solution of these molecules was dried onto a microscope coverslip (it can thus be assumed that $z_p = 0$ in the phase term of (4)), and imaged using a 100×, 1.45 NA, oil-immersion objective. At such an air/glass interface, highly characteristic diffraction patterns are observed, as shown in Fig. 4. We compare experimental measurements to images generated with the theoretical dipole diffraction model (1) using estimated orientations and positions. The results shown here were obtained after running the complete localization algorithm, and thus reflect super-resolved estimates. An accurate correspondence with the measurements is obtained, up to some residual aberrations visible around some of the Cy5 molecules.

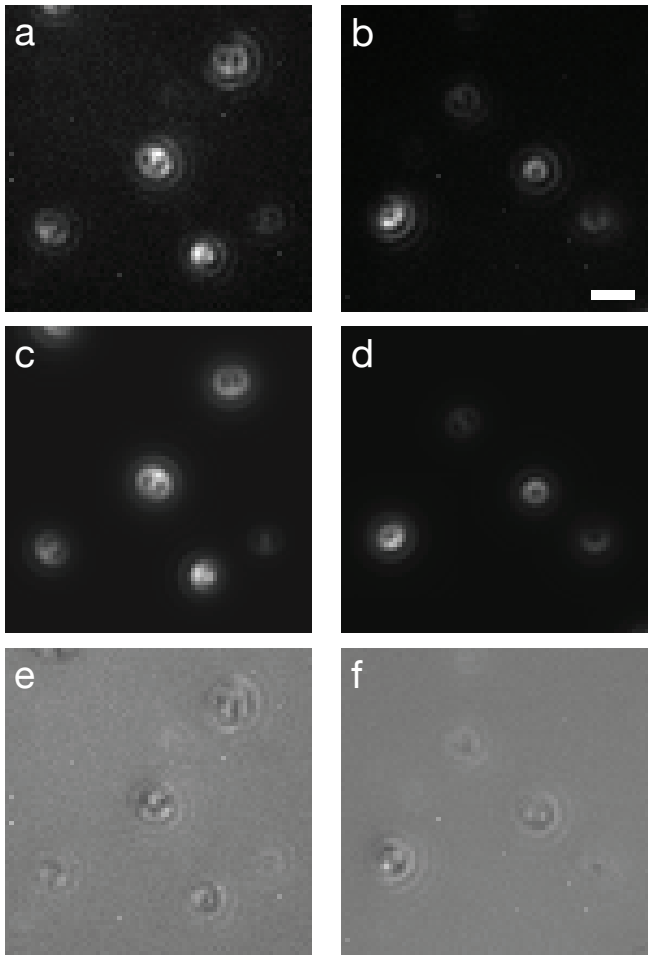

Fig. 4 (a-b) Dipole diffraction patterns for ssDNA-bound Cy5 molecules at an air/glass interface. (c-d) Rendered diffraction patterns using the positions and orientations estimated with the proposed algorithm. (e) error (a)-(c). (f) error (b)-(d). Scale bar: 1 μm.

6. REFERENCES

[1] E. Betzig, G. H. Patterson, R. Sougrat, O. W. Lindwasser, S. Olenych, J. S. Bonifacio, M. W. Davidson, J. Lippincott-Schwartz, and H. F. Hess, "Imaging intracellular fluorescent proteins at nanometer resolution," *Science*, vol. 313, pp. 1642–1645, 2006.

[2] M. J. Rust, M. Bates, and X. Zhuang, "Sub-diffraction-limit imaging by stochastic optical reconstruction microscopy (STORM)," *Nat. Methods*, vol. 3, no. 10, pp. 793–795, 2006.

[3] M. K. Cheezum, W. F. Walker, and W. H. Guilford, "Quantitative comparison of algorithms for tracking single fluorescent particles," *Biophys. J.*, vol. 81, no. 4, pp. 2378–2388, 2001.

[4] R. E. Thompson, D. R. Larson, and W. W. Webb, "Precise nanometer localization analysis for individual fluorescent probes," *Biophys. J.*, vol. 82, no. 5, pp. 2775–2783, 2002.

[5] J. Enderlein, E. Toprak, and P. R. Selvin, "Polarization effect on position accuracy of fluorophore localization," *Opt. Express*, vol. 14, no. 18, pp. 8111–8120, 2006.

[6] B. Huang, W. Wang, M. Bates, and X. Zhuang, "Three-dimensional super-resolution imaging by stochastic optical reconstruction microscopy," *Science*, vol. 319, pp. 810–813, 2008.

[7] F. Aguet, D. Van De Ville, and M. Unser, "A maximum-likelihood formalism for sub-resolution axial localization of fluorescent nanoparticles," *Opt. Express*, vol. 13, no. 26, pp. 10503–10522, 2005.

[8] W. T. Freeman and E. H. Adelson, "The design and use of steerable filters," *IEEE Trans. Pattern Anal. Mach. Intell.*, vol. 13, no. 9, pp. 891–906, 1991.

[9] S. F. Gibson and F. Lanni, "Experimental test of an analytical model of aberration in an oil-immersion objective lens used in three-dimensional light microscopy," *J. Opt. Soc. Am. A*, vol. 8, no. 10, pp. 1601–1613, 1991.

[10] F. Aguet, S. Geissbühler, I. Märki, T. Lasser, and M. Unser, "Super-resolution orientation estimation and localization of fluorescent dipoles using 3-D steerable filters," *Opt. Express*, vol. 17, no. 8, pp. 6829–6848, 2009.